Depopulation of subbands by magnetic and electric fields in gated $Al_xGa_{1-x}As$-GaAs quantum wells

K. Ensslin, D. Heitmann, and K. Ploog
Max-Planck-Institut für Festkörperforschung, Heisenbergstrasse 1, Postfach 80 06 65, D-7000 Stuttgart 80, West Germany
(Received 3 December 1987)

We have investigated the cyclotron resonance (CR) of selectively doped n-type $Al_xGa_{1-x}As$-GaAs quantum wells in which the carrier density could be tuned via a front-gate voltage V_g. With increasing V_g we observe a second CR which was found to represent the CR of a second subband E^1. The onset voltage V_{t1} and the occupation of the E^1 subband depend on the strength B of a perpendicular magnetic field. We found that the CR in the E^1 subband exhibits a lower effective mass and a significantly higher dynamic mobility as compared with the E^0 subband.

For the investigation of a two-dimensional electronic system (2DES) in heterostructures and quantum wells it is very useful if the 2D charge density N_S can be tuned in a reversible way.[1] We have prepared selectively doped n-type $Al_xGa_{1-x}As$-GaAs single-quantum-well structures where N_S could be varied by a frontgate voltage V_g from nearly zero up to high values of 9×10^{11} cm^{-2}. We have investigated cyclotron resonance (CR) excitation and with increasing V_g and N_S we observe the appearance of a second CR which represents the CR of a higher subband, E^1. The observation of several CR signals from different subbands is well known from investigations of the 2DES in narrow-gap materials.[2] To our knowledge this is the first observation in the $Al_xGa_{1-x}As$-GaAs system. The observed CR's in the two subbands are very sharp and well separated. Thus detailed information on dynamic mobilities, nonparabolicity, and subband occupation can be explored. We found that the onset V_{t1} for the occupation of the E^1 subband depends significantly on the strength B of a perpendicular magnetic field. We have investigated the origin of the magnetic depopulation both with CR and dc experiments. So far, magnetic depopulation has mainly been deduced from dc experiments. In most experiments the effect of parallel magnetic fields and the depopulation via the diamagnetic shift was discussed (e.g., Refs. 3 and 4), but also effects of purely perpendicular fields have been found.[5,6]

The samples were grown by molecular-beam epitaxy and have the following structure: a semi-insulating GaAs substrate, directly followed by a short period superlattice consisting of 10 periods of 2.5-nm AlAs and 2.5-nm GaAs, the active 50-nm GaAs well, a 3-nm spacer layer of $Al_xGa_{1-x}As$, a Si-doped 61-nm $Al_xGa_{1-x}As$ layer ($x=0.3$, $N_d\approx6\times10^{17}$ cm^{-3}), and an 8-nm GaAs cap layer. 5-nm NiCr gates with a 3-mm diameter were evaporated onto the sample. Outside the gate area Ohmic contacts were made to the 2D channel. The gate voltage V_g was applied between the frontgate and the channel. The carrier density N_S was determined *in situ* from magnetocapacitance-voltage (MCV) measurements (see below). The transmission T of far-infrared (FIR) radiation through the sample was measured with a Fourier-transform spectrometer which was connected via a waveguide system to a 14.5-T superconducting magnet. Spectra were taken at fixed N_S and B with **B** perpendicular to the sample plane. The temperature was 2.2 K. The resolution of the spectrometer was set to 0.1 cm^{-1}. More experimental details are included in Refs. 1 and 7. The latter emphasizes also the determination of N_S in gated heterostructures from magnetocapacitance and CR signal strength.

Figure 1 shows experimental spectra measured at fixed $B=9.6$ T for various V_g. With increasing V_g, and, correspondingly N_S, the strength of the CR signal increases. For $V_g=-0.3$ V the CR begins to broaden and for $V_g>-0.25$ V two resonances are observed. The higher frequency resonance has a significantly smaller linewidth. This resonance is identified in the following as a CR in the second subband, E^1.

In Fig. 2 we summarize some of our experimental results. We have measured CR at various values of B in series where V_g was varied in small increments of $\delta V_g=0.02$ V. To compare the experimental results for different B we express the resonance position ω_r in terms of an effective CR mass $m^*=eB/\omega_r$. For all B we have a general increase due to nonparabolicity. (It is so far not clear whether the increase of m^* at very small V_g is caused by localization effects[1,7] or intersubband coupling.[8] This needs further investigations by self-consistent band-structure calculation but is not important for the results here.) For a certain onset voltage V_{t1}, two CR's are resolved, as indicated in Fig. 2. This reflects the onset of the E^1-subband occupation. Inspection of Fig. 2 implies that V_{t1} depends significantly on B. The values of V_{t1} which have been determined from the onset of the CR splitting are plotted in Fig. 3 and are indicated by solid triangles.

For a further characterization of the samples we have performed quasi-dc experiments. We have measured the in-phase and 90°-phase (equal to differential capacitance, C-V) response of a small ac voltage (150 s^{-1}) that was superimposed to the gate voltage. For $B=0$ we observe the onset of the conductivity in the 2D channel at $V_{t0}=-0.90$ V. At $V_{t1}=-0.64$ V we observe a sudden

 ©1988 The American Physical Society

decrease of the conductivity which we attribute to the onset of intersubband scattering and therefore to the onset of the E^1 subband occupation. We also observe equivalent kinks in MCV which we can follow for nearly all magnetic fields. The position of these kinks is marked in Fig. 3 by open circles. For small fixed B we can observe Shubnikov–de Haas (SdH) -type oscillations of the E^0 subband which have different periodicities δV_g for $V_g < V_{t1}$ and $V_g > V_{t1}$. This allows us to determine the carrier density N_s^0 of the E^0 subband. It also gives us an independent method to determine the onset V_{t1} from the voltage where the periodicity changes (indicated by solid circles in Fig. 3). At some magnetic fields we can observe SdH-type oscillations from the E^1 subband at $\nu^1=1$ and $\nu^1=2$ and can thus also deduce, firstly, the onset voltage V_{t1} (indicated by squares in Fig. 3) and, secondly, the carrier density N_S^1 ($\nu^i=hN_s^i/eB$ denotes the filling factor in the ith subband). For other magnetic fields N_S^1 can be extracted from the relation $N_S=N_S^0+N_S^1$ since the total carrier density N_S, as extracted from V_g and sample capacitance, is known to vary only very little with magnetic fields. We see from Fig. 3 that all the different methods that we used here to determine V_{t1} provide consistent results in the overlapping B regimes.

For a further understanding of the system we have performed self-consistent subband calculations employing a numerical integration of the Schrödinger and Poisson equations. We use the known band-structure parameters and the geometry of the sample. The adjustable parameters are the donor concentration in the highly doped $Al_xGa_{1-x}As$ layer and the acceptor concentration in the

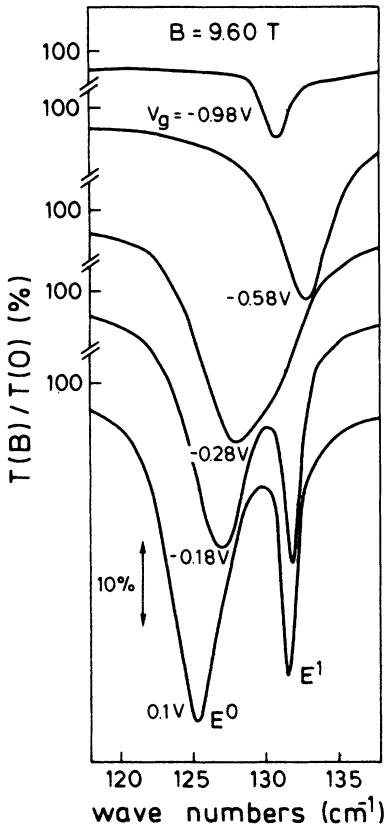

FIG. 1. Normalized transmission $T(B)/T(B=0)$ of unpolarized FIR radiation measured at fixed $B=9.6$ T for various gate voltages V_g. For $V_g > -0.25$ V two subbands E^0 and E^1 are occupied, which show different separated CR excitation.

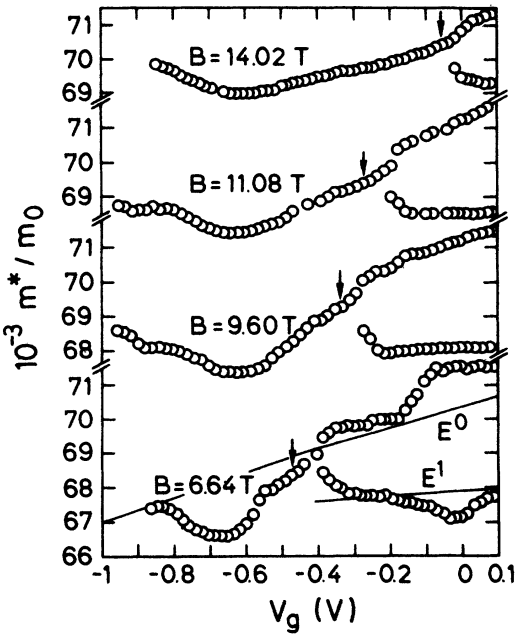

FIG. 2. Experimental resonance positions in terms of an effective mass m^* vs V_g at various magnetic fields B. For $B=6.6$ T the results of a self-consistent calculation are indicated by solid lines. The arrows indicate the position of $\nu^0=2$. For $\nu^0>2$ two subbands are occupied, where the energetical higher E^1 subband has the lower effective mass m^*.

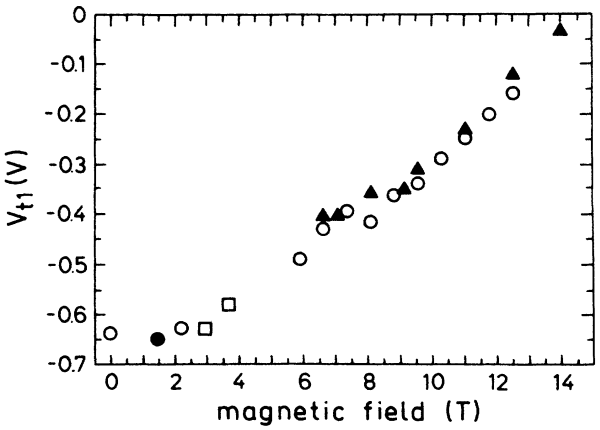

FIG. 3. Experimentally determined onset voltages V_{t1} for the occupation of the E^1 subband vs magnetic field. Values of V_{t1} are determined (a) from CR splitting [marked by solid triangles (▲)], (b) from the kink in MCV due to the onset of intersubband scattering [marked by open circles (○)], from the change in the SdH oscillation period of the E^0 subband [marked by solid circles (●)], and (d) from the SdH-type oscillations of the E^1 subband [marked by squares (□)].

unintentionally doped GaAs well. As a boundary condition on the substrate side of the structure we chose a vanishing derivative of the potential at the superlattice-substrate interface. We did not use the usual depletion approximation since there is no buffer layer in our structure. We did not include exchange and correlation effects. The calculation for $B=0$ gives the onset of the E^1-subband occupation at $V_{t1}=-0.60$ V in reasonable agreement with the experiment. The density $N_S^0(V_{t1})$ is then 2×10^{11} cm^{-1} corresponding to a subband spacing of 8.1 mV for V_{t1} and $B=0$.

Let us now explain the magnetic-field-induced subband depopulation as depicted in Fig. 3. We assume for a moment idealized conditions, i.e., δ-shaped Landau levels, no spin splitting, a constant CR mass m^*, N_S^1 in the E^1 subband to be small such that $\nu^1<1$, and no self-consistent effects on the subband separation due to an E^1 occupation. We denote the subband separation at N_S and $B=0$ by E_{10}. If, as shown schematically in Fig. 4, at a fixed density N_S^0 the magnetic field is varied, the Fermi energy $E_F(B)$ in the E^0 subband shows the well-known oscillations with discrete jumps at even values of ν^0. For B approaching zero, the Fermi energy $E_F(B)$ levels out at $E_F^0=E_F(N_S,B=0)=\pi\hbar^2N_S/m$. We can now distinguish different situations indicated by (a), (b), and (c) in Fig. 4. In the extreme case (a), where E_F^0 is smaller than the subband separation E_{10}, we find that for all B only the E^0 subband is occupied. This is the situation for small $V_g\le-0.65$ V in our experiments (see Figs. 2 and 3). In another extreme case, (c), $E_{10}\le\frac{1}{2}E_F^0$, we have the situation that for high B only the E^0 subband is occupied. For all $B<hN_S^0/2e$ (meaning $\nu^0>2$) both subbands are occupied. This is the case for $V_g\ge-0.05$ V in Figs. 2 and 3. In an intermediate case, $\frac{2}{3}E_F^0>E_{10}>\frac{1}{2}E_F^0$, we find that for such values of B that $\nu^0<2$ only E^0 is occupied. For $\nu^0>2$ and decreasing B we have a certain B regime where both subbands are occupied, then for still smaller B, again only the E^0 subband is occupied. For

$$[n/(n+1)]E_F^0>E_{10}>[(n-1)/n]E_F^0$$

we have several ($n=1,2,3,\ldots$) oscillations between a pure E^0 and a mixed E^0-E^1 occupation. If we translate this behavior into the representation of Fig. 3 then we expect that, for high B, the onset voltage V_{t1} should follow the condition $\nu^0=2=hN_S^0/eB$. This is indeed very well fulfilled for our experimental data (see also the arrows indicating $\nu^0=2$ in Fig. 2). From the idealized model above we would expect that with decreasing B in the moment, when subband separation and CR energy coincide, $\hbar\omega_c=\hbar eB/m^*=E_{10}$, the onset voltage jumps from a position corresponding to $N_S^0=2eB/h$ to $N_S^0=4eB/h$ and should then follow for $E_{10}m^*/\hbar e>B>E_{10}m^*/2\hbar e$ the condition $\nu^0=4$. This jump is indeed reflected in Fig. 3 by the structure and distinct offset of V_{t1} at $B_0\le8$ T. From this value of B_0 we can deduce that for these conditions, $B=8$ T, $N_S^0=3.9\times10^{11}$ cm^{-2}, the subband spacing is $E_{10}=13.8$ meV which is in agreement with our self-consistent band-structure calculations. In the idealized model we would expect at smaller B additional jumps of the onset voltage, when the conditions $n\hbar\omega_c=E_{10}$ ($n=2,3,\ldots$) occur.

Of course, the experimental situation is more complicated than the idealized model with respect to two points. (a) The subband spacing E_{10} is not constant but depends significantly on N_S^0 and V_g. In particular, the relevant subband separation for the threshold condition depends, since V_{t1} changes with B, self-consistently on B. (b) The finite width of the Landau levels is also important for the self-consistent arrangement of the subband energies. In particular, this applies for our gated quantum-well system, which has a relatively small subband spacing due to the strong bending of the bottom of the well. This is the reason why the jump of V_{t1} at $B_0=8$ T in Fig. 3 ($\hbar\omega_c=E_{10}$) is not so strongly pronounced in the experiment, as expected from the idealized model above. The additional jumps at smaller B for $n\hbar\omega_c=E_{10}$, $n=2,3,\ldots$, are smeared out. We hope to explain this behavior in more detail by more extensive self-consistent calculations including realistic Landau-level broadening. However, the main features of a depopulation of subbands by perpendicular magnetic fields, the pinning of the threshold voltage at the condition $\nu^0=2$ for high B and N_S^0, the jump of V_{t1} for $\hbar\omega_c=E_{10}$ and a leveling out at small B appear clearly in our experiment.

Let us now come back to CR in the case of two occupied subbands. Comparing the number of carriers that we determined from both, CR signal strength and MCV, we know that the high-frequency resonance with the corresponding lower mass in Fig. 2 is related to the E^1 subband. We have calculated m^{i*} for $B=0$ in the well-known approximation[2] $m^{i*}=m^*[1+4(\langle K\rangle_i+E_F-E_i)/E_g]^{1/2}$, where m^* is the band-edge mass, E_i is the

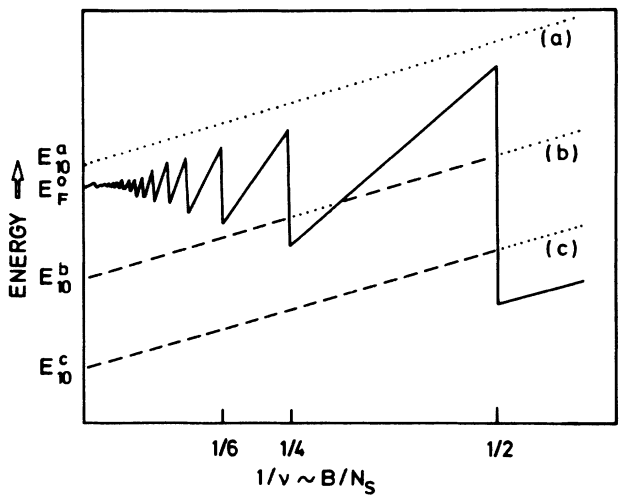

FIG. 4. Schematical representation of the Fermi energy in a magnetic field B if only the E^0 subband is occupied (solid line) and energy of the first Landau level in the second subband E^1 for different subband separation $E_{10}^a,E_{10}^b,E_{10}^c$. Dashed lines and dotted lines mark an occupied and an unoccupied E^1 subband, respectively.

subband energy, and E_g is the band-gap energy. The kinetic energy $\langle K \rangle_i$ was determined from the self-consistently calculated wave functions. The calculated results are included in Fig. 2 for $B=6.6$ T. They confirm the smaller mass for the E^1 subband and also the absolute values of m^{1*} and m^{2*}.

For the E^0 subband and $V_g > V_{t1}$, we observe that m^{0*} increases due to nonparabolicity, whereas m^{1*} remains nearly constant. The latter is consistent with a nearly constant value of N_S^1. We find indeed from the CR signal strength that, for $V_g \geq V_{t1}+0.05$ V, $N_S^1 \approx 1.5\times 10^{-11}$ cm^{-2} is nearly independent of V_g. An interesting feature is the sudden increase of m^{0*} for $V_g=-0.05$ V at $B=6.6$ T in Fig. 2. At this V_g, N_S^0 becomes 6.4×10^{11} cm^{-2} corresponding to a filling factor $\nu^0=4$. The onset for the occupation of the second Landau level leads to a significant change in the mass, as was discussed in Ref. 1. In addition, this onset also has an influence on the subband structure and changes in a self-consistent way also the E^1 wave function. The latter is reflected in the anomalous behavior of m^{1*} at the same gate voltage (see Fig. 2).

A final noteworthy point is the significantly smaller linewidth of the CR in the E^1 subband as compared with E^0. For example, for $B=9.6$ T and $V_g=0$ V the linewidths for E^1 correspond to an effective dynamic mobility $\mu_{\rm eff}=e\tau/m=300\,000$ cm^2/Vs compared with 100 000 cm^2/Vs for E^0 (τ denotes a scattering time which is extracted from the amplitude and linewidth of CR). In dc experiments one normally finds that above the occupation threshold μ decreases due to the onset of intersubband scattering.[9] Without a theoretical model it is not possible to extract E^1-related scattering processes from the dc conductivity due to the intrinsic coupling of both subbands. From our experiments we can determine separately dynamic mobilities for both subbands. However, for the E^1 subband we are always at low densities N_S^1, and are in the extreme quantum limit for those B, where we can reliably determine the CR half-width. In this situation one has found for systems with one occupied subband that the dynamic mobility was much larger (up to a factor of 5) than the dc mobility.[1,10] It is so far not exactly known how, in this case, $\mu_{\rm eff}$ is related to extrinsic or intrinsic processes that determine scattering and Landau-level width.

In summary, we have observed and explained the depopulation of electric subbands in selectively doped n-type $Al_xGa_{1-x}As$-GaAs quantum wells in perpendicular magnetic fields both in the CR and the dc behavior. The CR of the E^1 subband exhibits a smaller effective mass and higher dynamic mobility as compared with the E^0 subband.

We would like to thank U. Roessler for valuable discussion on subband calculation and acknowledge financial support by the Bundesministerium für Forschung und Technologie (Bonn, Germany).

[1]K. Ensslin, D. Heitmann, H. Sigg, and K. Ploog, Phys. Rev. B **36**, 8177 (1987).

[2]For a recent review see, e.g., U. Merkt, in *Festkörperprobleme (Advances in Solid State Physics)*, edited by P. Grosse (Vieweg, Braunschweig, 1987), Vol. 27, p. 109.

[3]R. E. Doezema, M. Nealon, and S. Whitmore, Phys. Rev. Lett. **45**, 1593 (1980).

[4]H. Reisinger and F. Koch, Surf. Sci. **170**, 397 (1986).

[5]J. C. Portal, R. J. Nicholas, M. A. Brummel, A. Y. Cho, K. Y. Cheng, and T. P. Pearsall, Solid State Commun. **43**, 907 (1982).

[6]M. A. Brummel, M. A. Hopkins, R. J. Nicholas, J. C. Portal, K. Y. Cheng, and A. Y. Cho, J. Phys. C **19**, L107 (1986).

[7]K. Ensslin, D. Heitmann, H. Sigg, and K. Ploog, in Proceedings of the Seventh International Conference on the Electronic Properties of Two-Dimensional Systems, Santa Fe, 1987 (unpublished); Surf. Sci. **196**, 263 (1988).

[8]Z. Schlesinger, J. C. M. Hwang, and S. J. Allen, Phys. Rev. Lett. **50**, 2098 (1983).

[9]H. L. Stoermer, A. C. Gossard, and W. Wiegmann, Solid State Commun. **41**, 707 (1982).

[10]M. J. Chou and D. C. Tsui, in Proceedings of the 7th International Conference on the Electronic Properties of Two-Dimensional Systems, Santa Fe, 1987 (unpublished); Surf. Sci. **196**, 279 (1988).